Determination of the Ionization Time Using Attosecond Photoelectron Interferometry

Jia Tan,[1] Yueming Zhou,[1,*] Mingrui He,[1] Yinbo Chen,[1] Qinghua Ke,[1] Jintai Liang,[1]
Xiaosong Zhu,[1] Min Li,[1,†] and Peixiang Lu[1,2,‡]

[1]*School of Physics and Wuhan National Laboratory for Optoelectronics, Huazhong University of Science and Technology, Wuhan 430074, China*

[2]*Hubei Key Laboratory of Optical Information and Pattern Recognition, Wuhan Institute of Technology, Wuhan 430205, China*

(Received 6 August 2018; revised manuscript received 21 October 2018; published 21 December 2018)

Laser-induced electron tunneling ionization from atoms and molecules plays as the trigger for a broad class of interesting strong-field phenomena in attosecond community. Understanding the time of electron tunneling ionization is vital to achieving the ultimate accuracy in attosecond metrology. We propose a novel attosecond photoelectron interferometer, which is based on the interference of the direct and near-forward rescattering electron wave packets, to determine the time information characterizing the tunneling process. Adding a weak perturbation in orthogonal to the strong fundamental field, the phases of the direct and the near-forward rescattering electron wave packets are modified, leading to the shift of the interferogram in the photoelectron momentum distributions. By analyzing the response of the interferogram to the perturbation, the real part of the ionization time, which denotes the instant when the electron exits the potential barrier, and the associated rescattering time are precisely retrieved. Moreover, the imaginary part of the ionization time, which has been interpreted as a quantity related to electron motion under the potential barrier, is also unambiguously determined.

DOI: 10.1103/PhysRevLett.121.253203

Tunneling is a fundamental process in quantum mechanisms and it has been used in many areas of science and technology, such as scanning tunneling microscopy, tunnel junction, tunnel diode, tunnel field-effect transistors, etc. In strong-field physics, electron tunneling from atoms or molecules by an intense laser pulse initiates a broad range of important phenomena in the ultrafast science community, such as high harmonic generation [1], high-order above threshold ionization [2], and enhanced multiple ionization [3–5]. Accurate information on the time of electron tunneling is central to achieving the ultimate accuracy in attosecond metrology. In the past decades, the questions of how long it takes the electron to tunnel through the potential barrier and when the electron appears in the outside of the potential barrier becomes a highly interesting and hotly controversial issue [6]. Recent progress in attosecond technology has allowed profound insight into the time of strong-field tunnel ionization [7–10].

Quantum mechanically, electron is described by wave function. In this point of view, the electron wave function extends from the inside to the outside of a potential barrier smoothly and continuously in the presence of the laser field [11]. There is a correspondence between the ionization time and the measured momentum of the photoelectrons and orders of the resultant harmonics. In many time-resolved experiments, the attosecond dynamics of a process is extracted based on this correspondence [12–19]. Theoretically, the ionization time has been conceptually defined in the quantum-orbit model [20], and the link between ionization time and the photoelectron momentum and harmonic order has been well established therein. This concept of ionization time has been tested in recent years [21,22]. With the advanced high-harmonic spectroscopy, the time where the electron exits the potential barrier and the associated rescattering time have been retrieved [22]. The results agree reasonably well with prediction of the quantum-orbit model. In the quantum-orbit model, the ionization time of tunneling is a complex number [20]. The real part of the ionization time represents when the electron emerges at the outside of the potential barrier. The imaginary part is interpreted to quantify the motion of the electron under the potential barrier [20,23–25]. In Ref. [22], only the real part of the ionization time was retrieved. Nevertheless, the imaginary part of the ionization time is especially important for many ultrafast processes. It has been pointed out that the imaginary part significantly affects the retrieval of the real part of the ionization time [26]. More remarkable, the imaginary time imprints a conspicuous phase on the tunneled electron wave packet and thus affects the interpretation of the interference in the photoelectron spectrum [27,28]. The imaginary time is also crucial for understanding the hotly discussed nonadiabatic effects in strong-field tunneling [25,29,30]. Very recently, with some assumptions on the real parts of the ionization time and the rescattering time, this imaginary ionization time was experimentally retrieved with the harmonic spectroscopy [31].

In this Letter, we demonstrate a novel attosecond photoelectron interferometer to retrieve both the real and

imaginary parts of the ionization time and the associated rescattering time. Our attosecond photoelectron interferometer is closely analogous to the traditional Michelson interferometer in optics. Strong-field tunneling ionization launches an electron wave packet. Part of this electron wave packet reaches the detector directly after tunneling and part experiences a near-forward rescattering. These two paths of the electron wave packet give rise to the interferogram in the photoelectron momentum distribution (PEMD) [32,33]. When a perturbation field in orthogonal to the fundamental driving field is introduced, the phase difference between these two paths changes, leading to the shift of the interference fringes in the PEMDs. By analyzing the response of the interference fringes in the PEMDs to the perturbation, the time information characterizing the paths of the electron wave packet can be determined. Our results show that the shift of interference fringes is very sensitive to the ionization time, especially the imaginary part. This enables us to extract the time information of tunneling precisely.

To demonstrate our scheme, we solve the time-dependent Schrödinger equation (TDSE) to obtain the PEMDs (atomic units are used throughout),

$$i\frac{\partial\Psi(\mathbf{r},t)}{\partial t}=\left[-\frac{\nabla^2}{2}+V(r)+\mathbf{r}\cdot\mathbf{E}(t)\right]\Psi(\mathbf{r},t), \quad (1)$$

where $V(r)=1/\sqrt{r^2+a^2}$ is the two-dimensional potential with $a=0.92$ to give the ionization potential of Xe ($I_p=0.446$ a.u.). $\mathbf{E}(t)=f(t)[F_x\cos(\omega t)\hat{\mathbf{e}}_x+F_y\cos(2\omega t+\varphi)\hat{\mathbf{e}}_y]$ is the electric field of the orthogonal two-color (OTC) pulses, which composes a fundamental pulse linearly polarized along the x axis and a second harmonic (SH) polarized along the y axis. ω is the frequency of the fundamental pulse and φ is the relative phase between the fundamental field and the SH. $f(t)$ is the envelope of the laser pulse, which has a trapezoidal shape, rising linearly during one cycle, then keeping constant for three cycles and decreasing linearly during the last one cycle of the fundamental pulse. In our scheme, the intensity of the SH is much weaker than the fundamental field (lower than 1%) and thus it can be treated as a small perturbation. This perturbation does not affect the tunneling of the electron wave packet but it disturbs the evolution of the electron wave packet, which induces a measurable observation in the PEMDs. This is essential in our scheme.

Figure 1 shows the PEMDs for strong-field tunneling ionization of Xe. Figure 1(a) displays the result for the 1600-nm single-color laser field and Figs. 1(b)–1(d) present the results by the OTC laser pulses. Three types of interference fringes are clearly observed. The ringlike structure, most visible in the low momentum part, is the above-threshold ionization peaks. The nearly vertical fringes are the interference of the direct electrons tunneling ionized during two adjacent half cycles [34,35]. Because of

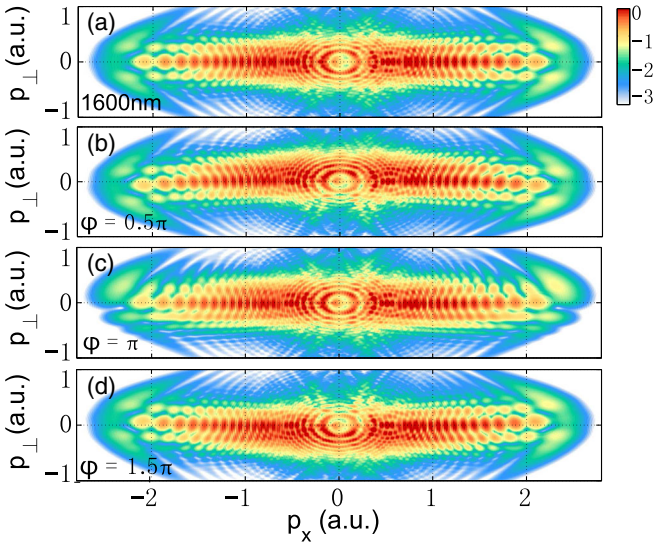

FIG. 1. PEMDs for tunneling ionization of Xe by a 1600 nm laser pulse (a) and the OTC fields (b)–(d). The intensity of the 1600 and 800 nm pulses are 1.5×10^{14} and 1.0×10^{12} W/cm^2, respectively. The relative phases of the OTC fields in (b)–(d) are 0.5π, π, and 1.5π, respectively.

the laser focal volume effect, these two types of interferences are usually unobservable in experiment for the laser wavelength in our calculations. The other nearly horizontal fringes are referred as the holographic structure originating from the interference of the electrons reaching the detector directly after tunneling and those with a near-forward rescattering with the parent ion [32,33]. This is the interference fringes we will focus on here. We should mention that this holographic interference has been observed in a broad range of experiments [32,36–39], and it is the most pronounced interference in the PEMDs for the near- and midinfrared laser pulses. For the single-color field, the holographic fringes are exactly symmetric about $p_\perp=0$. In the OTC fields, the two paths of the electrons undergoing are disturbed by SH field, resulting in the shift of fringes, as displayed in Figs. 1(b)–1(d). This shift and its dependence on the relative phases of the OTC field provide us time information about the electron tunneling through the potential barrier.

To reveal the disturbances of the SH on the holographic fringes more clearly, we wash out the vertical fringes by averaging the PEMDs over p_x with a window function [33] and several cuts at different p_x of the obtained PEMDs are shown in Figs. 2(a) and 2(b). The effect of the orthogonal perturbation on the interference fringes is obvious. At $p_x=-1.0$ a.u., the interference minima shift toward right and left with respect to the single-color field for $\varphi=0$ and $\varphi=\pi$, respectively. The shifts are reversed at $p_x=-1.6$ a.u..

The holographic interference is determined by the phase difference between the direct and the near-forward rescattering electrons. In the single-color field, the phase difference is written as [33,40]

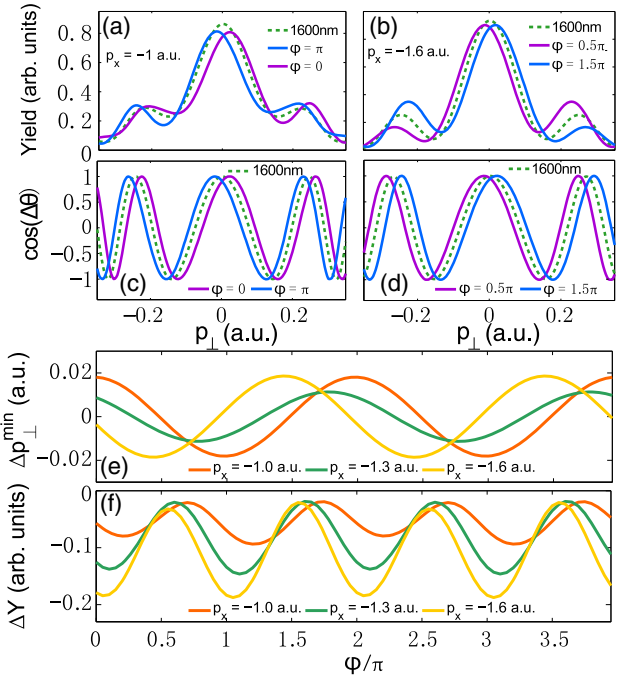

FIG. 2. Cuts of the averaged PEMDs for the single-color field (green dashed curve) and the OTC fields at (a) $p_x = -1.0$ and (b) $p_x = -1.6$ a.u. with different relative phases. (c), (d) The extracted interference term $\cos(\Delta\theta)$ as a function of p_y at the cut $p_x = -1.0$ and $p_x = -1.6$ a.u., respectively. (e) The shift $\Delta p_\perp^{\min}$ of the first minimum at $p_\perp > 0$ as a function of relative phase for cuts of $p_x = -1.0$ (orange curve), -1.3 (green curve), and -1.6 a.u. (yellow curve). (f) The change of the yield ΔY at $p_\perp = 0$ with respect to the single-color field as a function of the relative phase of the OTC fields at $p_x = -1.0$, -1.3, and -1.6 a.u..

$$\Delta\theta^{\mathrm{SC}} = \mathrm{Re}\left[\frac{1}{2}p_\perp^2(t_r - t_i^D)\right] + \alpha. \tag{2}$$

α represents the phase for the interaction between the rescattering electron and the parent ion [33]. $p_\perp$ denotes the final transverse momentum. The first term in the right-hand side accounts the phase difference accumulated during the propagation in the laser fields via the two different paths [40]. Only the real part of this term is responsible for the position of the interference fringes, while the imaginary part affects the relative yield of the direct and rescattering electrons and is irrelevant for the present study. t_i^D is the ionization time of the direct electron and t_r is the rescattering time. When a weak perturbative field was introduced, the phases for both paths are disturbed. Then the phase difference between the two paths reads [40]

$$\Delta\theta^{\mathrm{OTC}} = \mathrm{Re}\left[\frac{1}{2}\int_{t_i^D}^{t_r}[p_\perp + A_\perp(t;\varphi)]^2 dt\right] - \mathrm{Re}\left[\frac{1}{2}\int_{t_i^R}^{t_r}[k_\perp + A_\perp(t;\varphi)]^2 dt\right] + \alpha, \tag{3}$$

where $k_\perp = -[\int_{t_i^R}^{t_r} A_\perp(t;\varphi)dt/(t_r - t_i^R)]$ relating to the transverse momentum at recollision. $A_\perp(t;\varphi)$ is the vector potential of the SH and t_i^R is the ionization time of the rescattering electron. The direct and the rescattering electrons are ionized with different initial traverse momenta for the same measured final momentum $p_\perp$. In the OTC field, the initial transverse momentum of the direct electron is $p_\perp + A_\perp(t_i^D;\varphi)$ and it is $k_\perp + A_\perp(t_i^R;\varphi)$ for the rescattering electron. Because of this difference, the phases induced by the orthogonal perturbation during the propagation in the laser field are different for the direct and rescattering electrons [Eq. (3)], leading to the shift of the interference fringes in the PEMDs. Note that Eq. (3) degenerates into Eq. (2) when $A_\perp = 0$.

For the near-forward rescattering, the ionization time for the rescattering electron is approximately the same as the direct electron, $t_i^D \doteq t_i^R \doteq t_i$ [40]. Thus, the phase difference [Eq. (3)] in the OTC field reads [40],

$$\Delta\theta^{\mathrm{OTC}} = \mathrm{Re}\left[\frac{1}{2}(p_\perp - k_\perp)^2(t_r - t_i)\right] + \alpha. \tag{4}$$

Because of the perturbative nature of the SH, the phase α for the interaction of the ion and rescattering electron is the same for the single-color and our OTC fields. Then, by comparing Eqs. (2) and (4), we obtain that the holographic fringes are shifted by an amount of $\mathrm{Re}(k_\perp)$ due to the orthogonal perturbation. Obviously, the shift of the fringes depends on t_i and t_r. Thus, by monitoring this shift, the time information characterizing the interference paths can be retrieved.

We employ the procedure in Ref. [33] to extract the interference phase from PEMDs. The obtained term $\cos(\Delta\theta)$ is displayed in Figs. 2(c) and 2(d). To describe the shift of the interference fringes quantitatively, we monitor the position of the first interference minimum at $p_\perp > 0$ as a function of relative phase. Figure 2(e) displays the shift $\Delta p_\perp^{\min}$ of this minimum with respect to the single-color field as a function of the relative phase. It is shown that $\Delta p_\perp^{\min}$ modulates with relative phase, and it peaks at some certain φ, depending on p_x. For instance, $\Delta p_\perp^{\min}$ peaks at $\varphi = 2\pi$ for $p_x = -1.0$ a.u. and it peaks at $\varphi = 1.7\pi$ for $p_x = -1.3$ a.u.. Additionally, the amplitude of the modulation also depends on p_x, as shown in Fig. 2(e). We repeat this procedure for p_x ranging from -1.95–-0.75 a.u. The obtained $\Delta p_\perp^{\min}$ as a function of relative phase is shown in Fig. 3(a). It clearly indicates that the relative phase where $\Delta p_\perp^{\min}$ peaks varies with p_x.

The periodic oscillation of $\Delta p_\perp^{\min}$ suggests to us to fit it with $\Delta p_\perp^{\min} = P_m \cos(\varphi - \varphi_m)$, where P_m characterizes the amplitude of the oscillation and φ_m indicates the relative phase where the fringe shifts most from the single-color field. The obtained amplitude P_m and phase φ_m are displayed in Figs. 4(a) and 4(b), respectively. P_m and

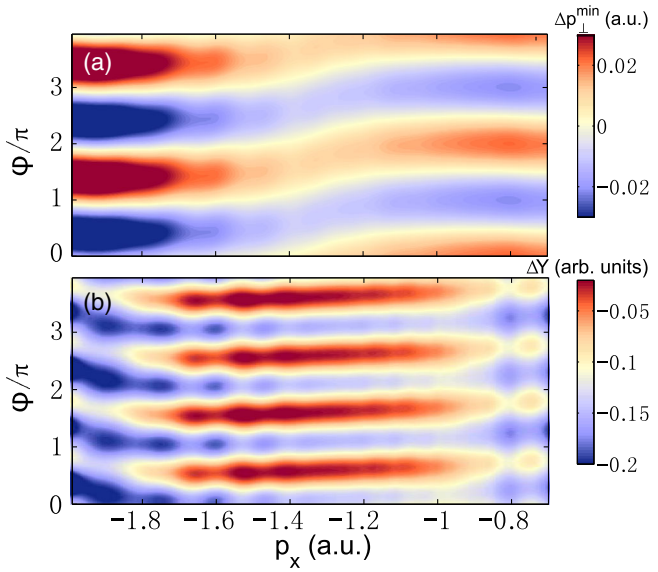

FIG. 3. (a) The shift $\Delta p_{\perp}^{\min}$ and (b) the relative yield ΔY as a function of relative phase for p_x ranging from $-1.95--0.75$ a.u.. These data are extracted from the TDSE results.

φ_m provide two independent observations to retrieve t_i and t_r. Note that t_i and t_r are complex numbers. For the rescattering time t_r, previous studies have demonstrated that the imaginary part is negligibly small [31,43] and thus it is a good approximation that the recollision time t_r is real. So there are three quantities to be retrieved. One more independent observation is needed.

The third observation can be obtained by monitoring the photoelectron yield at $p_{\perp} = 0$ [44,45]. In the single-color field, the yield maximizes at $p_{\perp} = 0$. In the OTC fields, the orthogonal perturbation streaks the yields away from $p_{\perp} = 0$ with an amount of $-A_{\perp}(t_i;\varphi)$. Hence, the yield in the OTC fields maximizes at $p_{\perp} = 0$ when the relative phase is chosen such that

$$\mathrm{Re}\{A_{\perp}[t_i(p_x);\varphi]\} = 0. \tag{5}$$

We trace the relative yield $\Delta Y = (Y^{\mathrm{OTC}} - Y^{\mathrm{SC}})/Y^{\mathrm{SC}}$ as a function of the relative phase, where Y^{OTC} and Y^{SC} are the ionization yields at $p_{\perp} = 0$ for the OTC and single-color fields, respectively. In Fig. 2(f), we show ΔY for different p_x. It clearly reveals that the relative phase at which ΔY peaks varies with p_x. Figure 3(b) shows ΔY over p_x ranging from $-1.95--0.75$ a.u. as a function of φ. The value of φ for maximal ΔY shifts gradually with p_x, implying the different ionization time for different p_x. We extract the relative phase where ΔY maximizes (denoted as δ_m). The results are shown in Fig. 4(c). This provides the third observation for determining t_i and t_r.

Before retrieving t_i and t_r, we first compare the measured quantities with those predicted by different models, i.e., the classical model [46], the quantum-orbit model [20],

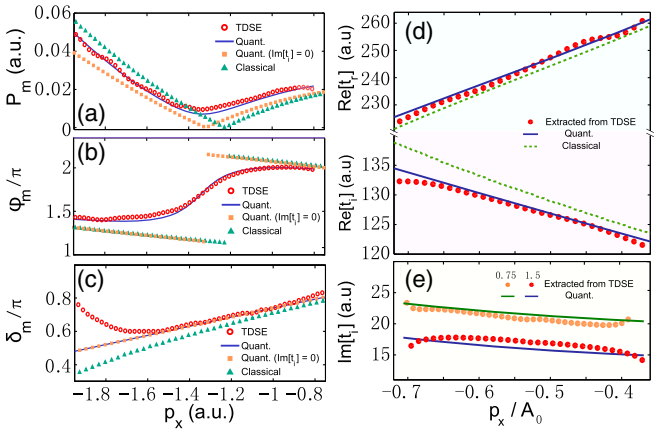

FIG. 4. (a) The oscillation amplitude P_m, (b) the phase φ_m where the shift $\Delta p_{\perp}^{\min}$ maximizes, and (c) the phase δ_m where the yield at $p_{\perp} = 0$ maximizes as a function of p_x. The circles, triangles, solid lines, and squares show the TDSE results, the results predicted by the classical model, the quantum-orbit model, and the quantum-orbit model with $\mathrm{Im}(t_i) = 0$, respectively. (d) Retrieved ionization times and recollision times. The dots show the results retrieved from TDSE data. The solid lines show the real parts of the quantum-orbit model times. The dashed lines represent the results from the classical model. (e) Retrieved tunneling times. The dots show the results from TDSE data. The results for two laser intensities $1.5I_0$ and $0.75I_0$ are shown ($I_0 = 1.0 \times 10^{14}$ W/cm^2). A_0 is the amplitude of the vector potential of the fundamental field ($A_0 = 2.3$ and 1.6 a.u. for $1.5I_0$ and $0.75I_0$, respectively).

and the quantum-orbit model with artificially setting $\mathrm{Im}(t_i) = 0$. For the classical model, the value of δ_m deviates obviously from the TDSE results, while the prediction from the quantum-orbit model agrees well with the TDSE results for p_x not close to the boundary. It is also indicated that the imaginary part of t_i does not affect δ_m, as shown in Fig. 4(c). For P_m [Fig. 4(a)], the TDSE results and the quantum-orbit model also agree excellently, and a minimum appears at $p_x = -1.32$ a.u.. While for the classical model, P_m deviates from the TDSE results seriously and the minimum shifts toward the right. For the quantum-orbit model with $\mathrm{Im}(t_i) = 0$, the position of the minimal P_m is coincidence with the TDSE results, but the value of P_m is significantly smaller. For φ_m, the difference between the TDSE results and the predictions of the different models is much more obvious. Only the predictions from the quantum-orbit model are in agreement with the TDSE results. For $\mathrm{Im}(t_i) = 0$, the results deviate seriously from the TDSE data as shown in Fig. 4(b). This indicates the sensitivity of the observation φ_m to the imaginary part of the ionization time.

The retrieved real part of the ionization time and the associated rescattering time are shown in Fig. 4(d). Both of them match well with the quantum-orbit model while they deviate distinctly from the classical model. We mention that in previous studies of retrieving the ionization and

rescattering times with harmonic spectroscopy, a zero or Keldysh time for the imaginary part of t_i was assumed [22,26]. In our scheme, no such assumption is made and the imaginary part is treated as an unknown quantity. The retrieved $\mathrm{Im}(t_i)$ is shown in Fig. 4(e). It decreases as p_x moves towards zero. This is easy to understand. For p_x more close to zero, the instantaneous electric field at tunneling increases, and thus the width and height of the potential barrier decrease, leading to the decreasing of the imaginary part of t_i. Our retrieved results agree well with the value from the quantum-orbit model. In Fig. 4(e), we also show the retrieved $\mathrm{Im}(t_i)$ at a weaker laser intensity. As expected, $\mathrm{Im}(t_i)$ becomes larger for lower laser intensity.

In the view of the quantum orbit, the imaginary ionization time quantifies the motion of the electron under the potential barrier [23,24,47]. It significantly influences the prediction of the quantum-orbit model on the PEMDs [27,28]. Thus, determination of this imaginary time is prerequisite for accurate information retrieval from the PEMDs, which has become a routine method for probing ultrafast electron dynamics in atoms and molecules. Moreover, there are many elusive nonadiabatic features in strong-field tunneling ionization. Revealing the nonadiabatic properties of strong-field tunneling ionization is fundamentally interesting in the attosecond science. The imaginary time is a crucial quantity to quantify these nonadiabatic effects [47,48]. Our scheme provides a particularly accurate and experimentally feasible way to measure this quantity.

In conclusion, we demonstrated an attosecond photoelectron interferometry to probe the detailed properties of the electron tunneling through the potential barrier. We have shown that the ionization time, both the real and imaginary parts, as well as the rescattering time can be retrieved by monitoring the interference fringes in the PEMDs. This provides the time map for the momentum-resolved photoelectron spectrum. Our results show that the interference fringes are particularly sensitive to the imaginary part of the ionization time. This imaginary time is closely related to the nonadiabtic effect in tunneling [23,24,47,48]. Thus, our interferometry should be efficient in exploring the nonadiabatic properties in strong-field tunneling ionization.

In attosecond science, the photoelectron interferometer is an extensively used method in probing the ultrafast electron dynamics [18,19,49]. However, the Coulomb interaction could significantly affect the interferogram, which complexes information extraction. In our scheme, one can be free from handling the Coulomb influence by monitoring the response of the interference fringes to a weak perturbation. This advantage allows us to retrieve dynamic information from the interference fringes precisely. It may provide a feasible tool for probing the subtle multielectron effect in more complex systems with attosecond temporal resolution.

Y. Zhou gratefully acknowledges Professor Manfred Lein for his helpful discussion and suggestion. This work was supported by the National Natural Science Foundation of China (11622431, 11874163, 61475055, 11604108, 11627809) and the Program for HUST Academic Frontier Youth Team.

*Corresponding author.
zhouymhust@hust.edu.cn
†Corresponding author.
mli@hust.edu.cn
‡Corresponding author.
lupeixiang@hust.edu.cn

[1] F. Krausz and M. Ivanov, Attosecond physics, Rev. Mod. Phys. **81**, 163 (2009).
[2] W. Becker, F. Grasbon, R. Kopold, D. B. Miloševic, G. G. Paulus, and H. Walther, Above-threshold ionization: From classical features to quantum effect, Adv. At. Mol. Opt. Phys. **48**, 35 (2002).
[3] W. Becker, X. Liu, P. J. Ho, and J. H. Eberly, Theories of photoelectron correlation in laser-driven multiple atomic ionization, Rev. Mod. Phys. **84**, 1011 (2012).
[4] T. Weber, H. Giessen, M. Weckenbrock, G. Urbasch, A. Staudte, L. Spielberger, O. Jagutzki, V. Mergel, M. Vollmer, and R. Dörner, Correlated electron emission in multiphoton double ionization, Nature (London) **405**, 658 (2000).
[5] Y. Zhou, Q. Liao, and P. Lu, Asymmetric electron energy sharing in strong-field double ionization of helium, Phys. Rev. A **82**, 053402 (2010).
[6] E. H. Hauge and J. A. Støvneng, Tunneling times: A critical review, Rev. Mod. Phys. **61**, 917 (1989).
[7] P. Eckle, A. N. Pfeiffer, C. Cirelli, A. Staudte, R. Dörner, H. G. Muller, M. Büttiker, and U. Keller, Attosecond ionization and tunneling delay time measurements in helium, Science **322**, 1525 (2008).
[8] A. N. Pfeiffer, C. Cirelli, M. Smolarski, D. Dimitrovski, M. Abu-samha, L. B. Madsen, and U. Keller, Attoclock reveals natural coordinates of the laser-induced tunneling current flow in atoms, Nat. Phys. **8**, 76 (2012).
[9] N. Camus, E. Yakaboylu, L. Fechner, M. Klaiber, M. Laux, Y. Mi, K. Z. Hatsagorsyan, T. Pfeifer, C. H. Keitel, and R. Moshammer, Experimental Evidence for Quantum Tunneling Time, Phys. Rev. Lett. **119**, 023201 (2017).
[10] L. Torlina, F. Morales, J. Kaushal, I. Ivanov, A. Kheifets, A. Zielinski, A. Scrinzi, H. G. Muller, S. Sukiasyan, M. Ivanov, and O. Smirnova, Interpreting attoclock measurements of tunneling times, Nat. Phys. **11**, 503 (2015).
[11] M. Lein, Electrons get real, Nature (London) **485**, 313 (2012).
[12] S. Baker, J. S. Robinson, C. A. Haworth, H. Teng, R. A. Smith, C. C. Chirilă, M. Lein, J. W. G. Tisch, and J. P. Marangos, Probing proton dynamics in molecules on an attosecond time scale, Science **312**, 424 (2006).
[13] W. Li, X. Zhou, R. Lock, S. Patchkovskii, A. Stolow, H. Kapteyn, and M. Murnane, Time-resolved dynamics in N_2O_4 probed using high harmonic generation, Science **322**, 1207 (2008).

[14] B. McFarland, J. Farrell, P. Bucksbaum, and M. Guhr, High harmonic generation from multiple orbitals in N_2, Science **322**, 1232 (2008).
[15] O. Smirnova, Y. Mairesse, S. Patchkovskii, N. Dudovich, D. Villeneuve, P. Corkum, and M. Y. Ivanov, High harmonic interferometry of multi-electron dynamics in molecules, Nature (London) **460**, 972 (2009).
[16] P. Kraus, B. Mignolet, D. Baykusheva, A. Rupenyan, L. Horný, E. Penka, G. Grassi, O. Tolstikhin, J. Schneider, F. Jensen, L. Madsen, A. Bandrauk, F. Remacle, and H. Wörner, Measurement and laser control of attosecond charge migration in ionized iodoacetylene, Science **350**, 790 (2015).
[17] P. Lan, M. Ruhmann, L. He, C. Zhai, F. Wang, X. Zhu, Q. Zhang, Y. Zhou, M. Li, M. Lein, and P. Lu, Attosecond Probing of Nuclear Dynamics with Trajectory-Resolved High-Harmonic Spectroscopy, Phys. Rev. Lett. **119**, 033201 (2017).
[18] X. Xie, S. Roither, D. Kartashov, E. Persson, D. G. Arbó, L. Zhang, S. Gräfe, M. S. Schöffler, J. Burgdörfer, Andrius Baltuška, and M. Kitzler, Attosecond Probe of Valence-Electron Wave Packets by Subcycle Sculpted Laser Fields, Phys. Rev. Lett. **108**, 193004 (2012).
[19] M. Haertelt, X. Bian, M. Spanner, A. Staudte, and P. Corkum, Probing Molecular Dynamics by Laser-Induced Backscattering Holography, Phys. Rev. Lett. **116**, 133001 (2016).
[20] P. Salières, B. Carré, L. L. Déroff, F. Grasbon, G. G. Paulus, H. Walther, R. Kopold, W. Becker, D. B. Milošević, A. Sanpera, and M. Lewenstein, Feynman's path-integral approach for intense-laser-atom interactions, Science **292**, 902 (2001).
[21] J. M. Dahlström, A. L'Huillier, and J. Mauritsson, Quantum mechanical approach to probing the birth of attosecond pulses using a two-color field, J. Phys. B **44**, 095602 (2011).
[22] D. Shafir, H. Soifer, B. D. Bruner, M. Dagan, Y. Mairesse, S. Patchkovskii, M. Y. Ivanov, O. Smirnova, and N. Dudovich, Resolving the time when an electron exits a tunneling barrier, Nature (London) **485**, 343 (2012).
[23] L. V. Keldysh, Ionization in the field of a strong electromagnetic wave, J. Exp. Theor. Phys. **20**, 1307 (1965).
[24] A. M. Perelomov, V. S. Popov, and M. V. Terent'ev, Ionization of atoms in an alternating electric field: II, J. Exp. Theor. Phys. **24**, 207 (1967).
[25] M. Ivanov, M. Spanner, and O. Smirnova, Anatomy of strong field ionization, J. Mod. Opt. **52**, 165 (2005).
[26] J. Zhao and M. Lein, Determination of Ionization and Tunneling Times in High-Order Harmonic Generation, Phys. Rev. Lett. **111**, 043901 (2013).
[27] T. Yan and D. Bauer, Sub-barrier Coulomb effects on the interference pattern in tunneling-ionization photoelectron spectra, Phys. Rev. A **86**, 053403 (2012).
[28] M. Han, P. Ge, Y. Shao, M. Liu, Y. Deng, C. Wu, Q. Gong, and Y. Liu, Revealing the Sub-Barrier Phase using a Spatiotemporal Interferometer with Orthogonal Two-Color Laser Fields of Comparable Intensity, Phys. Rev. Lett. **119**, 073201 (2017).
[29] G. Yudin and M. Ivanov, Nonadiabatic tunnel ionization: Looking inside a laser cycle, Phys. Rev. A **64**, 013409 (2001).
[30] M. Li, J. Geng, M. Han, M. Liu, L. Peng, Q. Gong, and Y. Liu, Subcycle nonadiabatic strong-field tunneling ionization, Phys. Rev. A **93**, 013402 (2016).
[31] O. Pedatzur, G. Orenstein, V. Serbinenko, H. Soifer, B. D. Bruner, A. J. Uzan, D. S. Brambila, A. G. Harvey, L. Torlina, F. Morales, O. Smirniva, and N. Dudovich, Attosecond tunneling interferometry, Nat. Phys. **11**, 815 (2015).
[32] Y. Huismans, A. Rouzée, A. Gijsbertsen, J. Jungmann, A. Smolkowska, P. Logman, F. Lépine, C. Cauchy, S. Zamith, T. Marchenko, J. Bakker, G. Berden, B. Redlich, A. van der Meer, H. Muller, W. Vermin, K. Schafer, M. Spanner, M. Ivanov, O. Smirnova *et al.*, Time-resolved holography with photoelectrons, Science **331**, 61 (2011).
[33] Y. Zhou, O. I. Tolstikhin, and T. Morishita, Near-Forward Rescattering Photoelectron Holography in Strong-Field Ionization: Extraction of the Phase of the Scattering Amplitude, Phys. Rev. Lett. **116**, 173001 (2016).
[34] F. Lindner, M. G. Schätzel, H. Walther, A. Baltuška, E. Goulielmakis, F. Krausz, D. B. Milošević, D. Bauer, W. Becker, and G. G. Paulus, Attosecond Double-Slit Experiment, Phys. Rev. Lett. **95**, 040401 (2005).
[35] M. Richter, M. Kunitski, M. Schöffler, T. Jahnke, L. P. H. Schmidt, M. Li, Y. Liu, and R. Dörner, Streaking Temporal Double-Slit Interference by an Orthogonal Two-Color Laser Field, Phys. Rev. Lett. **114**, 143001 (2015).
[36] D. Hickstein, P. Ranitovic, S. Witte, X. Tong, Y. Huismans, P. Arpin, X. Zhou, K. Keister, C. Hogle, B. Zhang, C. Ding, P. Johnsson, N. Toshima, M. Vrakking, M. Murnane, and H. Kapteyn, Direct Visualization of Laser-Driven Electron Multiple Scattering and Tunneling Distance in Strong-Field Ionization, Phys. Rev. Lett. **109**, 073004 (2012).
[37] M. Meckel, A. Staudte, S. Patchkovskii, D. Villeneuve, P. Corkum, R. Dörner, and M. Spanner, Signatures of the continuum electron phase in molecular strong-field photoelectron holography, Nat. Phys. **10**, 594 (2014).
[38] D. G. Arbó, C. Lemell, S. Nagele, N. Camus, L. Fechner, A. Krupp, T. Pfeifer, S. D. López, R. Moshammer, and J. Burgdörfer, Ionization of argon by two-color laser pulses with coherent phase control, Phys. Rev. A **92**, 023402 (2015).
[39] L. Fechner, N. Camus, A. Krupp, J. Ullrich, T. Pfeifer, and R. Moshammer, Creation and survival of autoionizing states in strong laser fields, Phys. Rev. A **92**, 051403(R) (2015).
[40] See Supplemental Material at http://link.aps.org/supplemental/10.1103/PhysRevLett.121.253203 for details about the phase in our interferometer, which includes Refs. [41,42].
[41] G. Porat, G. Alon, S. Rozen, O. Pedatzur, M. Krger, D. Azoury, A. Natan, G. Orenstein, B. Bruner, M. Vrakking, and N. Dudovich, Attosecond time-resolved photoelectron holography, Nat. Commun. **9**, 2805 (2018).
[42] H. Xie, M Li, S. Luo, Y. Li, J. Tan, Y. Zhou, W. Cao, and P. Lu, Photoelectron holography and forward scattering in atomic ionization by elliptically polarized laser pulses, Opt. Lett. **43**, 3220 (2018).
[43] E. V. van der Zwan and M. Lein, Molecular Imaging Using High-Order Harmonic Generation and Above-Threshold Ionization, Phys. Rev. Lett. **108**, 043004 (2012).

[44] J. Henkel and M. Lein, Analysis of electron trajectories with two-color strong-field ionization, Phys. Rev. A **92**, 013422 (2015).

[45] N. Eicke and M. Lein, Extracting trajectory information from two-color strong-field ionization, J. Mod. Opt. **64**, 981 (2017).

[46] P. B. Corkum, Plasma Perspective on Strong Field Multiphoton Ionization, Phys. Rev. Lett. **71**, 1994 (1993).

[47] V. D. Mur, S. V. Popruzhenko, and V. S. Popov, Energy and Momentum Spectra of Photoelectrons under Conditions of Ionization by Strong Laser Radiation (the Case of Elliptic Polarization), J. Exp. Theor. Phys. **92**, 777 (2001).

[48] I. Barth and O. Smirnova, Nonadiabatic tunneling in circularly polarized laser fields. II. Derivation of formulas, Phys. Rev. A **87**, 013433 (2013).

[49] M. He, Y. Li, Y. Zhou, M. Li, W. Cao, and P. Lu, Direct Visualization of Valence Electron Motion Using Strong-Field Photoelectron Holography, Phys. Rev. Lett. **120**, 133204 (2018).